J. Fluid Mech. (1999), *vol.* 390, *pp.* 223–249. Printed in the United Kingdom

Experimental studies of strongly stratified flow past three-dimensional orography

By S. B. VOSPER[1], I. P. CASTRO[2], W. H. SNYDER[2] AND S. D. MOBBS[1]

[1]The Environment Centre, University of Leeds, Leeds LS2 9JT, UK

[2]School of Mechanical and Materials Engineering, University of Surrey, Guildford GU2 5XH, UK

(Received 20 July 1998 and in revised form 7 January 1999)

Stably stratified flows past three-dimensional orography have been investigated using a stratified towing tank. Flows past idealized axisymmetric orography in which the Froude number, $F_h = U/Nh$ (where U is the towing speed, N is the buoyancy frequency and h is the height of the obstacle) is less than unity have been studied. The orography considered consists of two sizes of hemisphere and two cones of different slope. For all the obstacles measurements show that as F_h decreases, the drag coefficient increases, reaching between 2.8 and 5.4 times the value in neutral flow (depending on obstacle shape) for $F_h \lesssim 0.25$. Local maxima and minima in the drag also occur. These are due to the finite depth of the tank and can be explained by linear gravity-wave theory. Flow visualization reveals a lee wave train downstream in which the wave amplitude is $O(F_h h)$, the smallest wave amplitude occurring for the steepest cone. Measurements show that for all the obstacles, the dividing-streamline height, z_s, is described reasonably well by the formula $z_s/h = 1 - F_h$. Flow visualization and acoustic Doppler velocimeter measurements in the wake of the obstacles show that vortex shedding occurs when $F_h \lesssim 0.4$ and that the period of the vortex shedding is independent of height. Based on velocity measurements in the wake of both sizes of hemisphere (plus two additional smaller hemispheres), it is shown that a blockage-corrected Strouhal number, $S_{2_c} = fL_2/U_c$, collapses onto a single curve when plotted against the effective Froude number, $F_{h_c} = U_c/Nh$. Here, U_c is the blockage-corrected free-stream speed based on mass-flux considerations, f is the vortex shedding frequency and L_2 is the obstacle width at a height $z_s/2$. Collapse of the data is also obtained for the two different shapes of cone and for additional measurements made in the wake of triangular and rectangular flat plates. Indeed, the values of S_{2_c} for all these obstacles are similar and this suggests that despite the fact that the obstacle widths vary with height, a single length scale determines the vortex-street dynamics. Experiments conducted using a splitter plate indicate that the shedding mechanism provides a major contribution to the total drag ($\sim 25\%$). The addition of an upstream pointing 'verge region' to a hemisphere is also shown to increase the drag significantly in strongly stratified flow. Possible mechanisms for this are discussed.

1. Introduction

Stably stratified atmospheric flows over orography have been the subject of extensive research. One of the main reasons for the interest in this subject is that many of the features of orographic flows occur on scales which are too small to be resolved by

current numerical weather prediction and general circulation models. Since some of these features give rise to a net drag force on the orography (and hence a retarding force on the mean atmospheric flow), there is a need to parametrize their effects in the larger scale numerical models. Early parametrization schemes were designed to include the effects of the unresolved gravity waves generated by the flow over mountain ranges (e.g. Palmer, Shutts & Swinbank 1986) and more recently these schemes have been refined in order to represent other effects such as low-level wake drag (Lott & Miller 1997). In order to improve local weather forecasts there is also a need to understand the mechanisms which give rise to other features of orographic flows (e.g. intense downslope windstorms, lee vortex formation). Apart from the improvement of numerical weather prediction there are other reasons why a good understanding of stably stratified orographic flows is important. For example, before reliable pollution dispersion predictions in hilly terrain can be made a better understanding of the flow is required (e.g. Snyder & Hunt 1984).

An important parameter that influences the gross features of flow over orography under stratified conditions is $F_h = U/Nh$, commonly referred to as a Froude number, where U is the undisturbed air-stream speed, N is the buoyancy frequency and h is the mountain height. Note that the term Froude number is usually reserved for ratios of wave speeds to flow speeds and F_h clearly does not represent such a ratio. In the interests of remaining consistent with previous authors and to avoid further confusion we shall, however, continue to use this terminology and will refer to F_h as a Froude number.

Weakly stratified flows ($F_h > 1$) are quite well understood because when the slope of the terrain is sufficiently small the governing equations can be linearized to a good degree of approximation (e.g. Smith 1988). However, more strongly stratified flows ($F_h < 1$) tend to be far more complicated and nonlinear effects are important. Although much progress has recently been made towards a greater understanding of these flows, questions such as how the drag varies with F_h and what mechanisms are responsible for the drag when F_h is considerably smaller than unity are still far from being answered completely. Broadly speaking, flows for which $F_h \ll 1$ tend to be around the mountain and only streamlines which originate at levels sufficiently close to the summit height will pass over the mountain. Based on simple energy arguments Sheppard (1956) predicted that only fluid parcels which originate at a height greater than $h(1-F_h)$ would pass over the summit and that below this height the streamlines would go around the mountain. Further theoretical advances were made by Drazin (1961). His theory for inviscid stably stratified flow past three-dimensional orography is asymptotic for small F_h and to lowest order it predicts that the flow is in horizontal planes around the orography. The streamlines are deflected a tiny amount, $O(F_h^2 h)$, as they pass the orography and this is caused by the vertical variation in the pressure due to the change of the terrain's cross-section with height. Drazin's solution, being inviscid, does not allow for the possibility of separation from the obstacle. It also breaks down at the summit of the orography where the fluid is able to pass over the top. This 'summit region' extends to a depth of $O(F_h h)$ below the summit and is a region of gravity-wave generation. Recently Hunt *et al.* (1997) have attempted to match the flow above the summit (using an approximate solution based on linear theory) to the Drazin solution below in the 'middle region' of the flow. There is also another region in which the Drazin solution breaks down and this occurs at the foot of mountains (Hunt & Snyder 1980) whose shapes are such that they do not abruptly descend into the plane, but rather blend into the ground gradually. This 'verge region' again has a depth of $O(F_h h)$ and recent theoretical work by Greenslade

(1994) indicates that vertical motion occurs within this region, suggesting that this is another region of gravity-wave generation. The question of how far these gravity waves propagate (e.g. can they propagate into the middle region?) and whether or not they make a significant contribution to the net drag remains an open one.

With the recent acceleration in computing technology numerical simulation of three-dimensional orographic flows has become possible (e.g. Smolarkiewicz & Rotunno 1989; Miranda & James 1992; Schar & Durran 1997). Numerical simulation provides a powerful technique for understanding these very complicated flows but cannot provide complete answers. An equally powerful and complementary approach is one of laboratory experiment. Despite the vastly different scales (and hence Reynolds number) much insight into atmospheric flows has been gained through experiments conducted in the laboratory. In particular, Brighton (1978), using a recirculating stratified tank, studied strongly stratified flows past three-dimensional obstacles. When $F_h \ll 1$ his experiments revealed flows in which the fluid trajectories were around the obstacles and were almost horizontal (except near the summits), in qualitative agreement with Drazin's theory. Two features of the flows which could not be explained by Drazin's theory, however, were a horizontally orientated cow-horn shaped eddy which occurred for $F_h \lesssim 1$ and an unsteady separated wake in which vortices were shed periodically. The vortex shedding occurred when $F_h < 0.15$. Hunt & Snyder (1980) used a large towing tank to examine the flow structure over a three-dimensional bell-shaped hill. Again, in agreement with Drazin's solution they found that away from the summit and the base of the orography, the flow was more or less horizontal. As in Brighton's (1978) experiments, however, the flow was seen to separate from the sides of the obstacle below the summit region. Castro, Snyder & Marsh (1983) studied stratified flows past three-dimensional triangular ridges of various widths in a towing tank. Their experiments also revealed a separated unsteady wake. Vortex shedding was observed for $F_h \leqslant 0.3$ although the wake was still unsteady for values of F_h as high as 0.4, at which point the wake exhibited a 'meandering' behaviour.

Much attention has been devoted to the 'dividing-streamline height' concept in stratified towing-tank work. By the dividing-streamline height we refer to the height from which a fluid parcel must originate far upstream if it is to pass over the orography rather than travel around it. Sheppard's (1956) energy-based arguments indicate that, to a first approximation, for flows in which $F_h < 1$ the dividing-streamline height, z_s, is given by

$$z_s/h = (1 - F_h). \tag{1.1}$$

Smith (1988), in a linearized analytical study, points out that this formula takes no account of the dynamic pressure perturbation. Nevertheless, Sheppard's formula has been shown to work quite well (e.g. Hunt & Snyder 1980; Snyder, Britter & Hunt 1980), at least for obstacles of low spanwise aspect ratio. Towing-tank studies conducted by Snyder *et al.* (1985) with truncated sinusoidal ridges orientated at various angles to the flow and the three-dimensional ridge experiments presented by Castro *et al.* (1983) suggest that Sheppard's criterion for a fluid parcel to travel over the summit is a necessary condition rather than a sufficient one. Indeed, depending on the geometry of the obstacle, fluid parcels which originate just off the centreplane may travel around the sides regardless of whether they possess enough kinetic energy to pass over the summit.

Despite the obvious potential of the laboratory approach only a handful of experiments have been designed to measure orographic drag. Lofquist & Purtell (1984) described experiments in which the drag on spheres was measured in a tank over

a range of Froude and Reynolds numbers. Similar work was undertaken by Mason (1977) who measured the drag on a sphere under stratified conditions in both rotating and non-rotating cases. The application of both these studies to atmospheric flow is, of course, limited by the fact that the measurements were for obstacles which were remote from boundaries. Castro, Snyder & Baines (1990) made drag measurements which are more relevant to the atmospheric case by surface mounting the obstacles. Using a towing-tank facility they made measurements of the drag exerted on two-dimensional and three-dimensional hills and fences for values of $F_h \gtrsim 0.5$. Their results indicate a dependence of the drag on the parameter $K = ND/\pi U$, where D is the fluid depth. Local minima in the drag occur at integer values of K with maxima occurring in between. This is entirely consistent with linear theory for stratified flow in a channel of finite depth. The effect of the rigid-lid boundary condition caused by the bottom of the tank is to restrict the number of gravity-wave modes to a finite number, Int(K). Under certain conditions the drag on these obstacles was unsteady and varied periodically during the tows. These oscillations were shown to be directly linked to periodic oscillations in the gravity-wave amplitude and have only more recently been satisfactorily explained (Rottman, Broutman & Grimshaw 1996).

There is extensive literature on stratified flows over two-dimensional orography and it is perhaps appropriate to discuss these flows here and highlight the differences and similarities between two- and three-dimensional flows. One major difference is that, unlike the three-dimensional case, in two-dimensional flow fluid parcels which originate upstream below the dividing-streamline height cannot pass around the mountain and instead may become completely blocked upstream. This flow blocking is controlled by the presence of columnar modes which propagate horizontally upstream (Baines & Hoinka 1985). These modes presumably exist in three-dimensional flow also, but are likely to be of smaller amplitude. For sufficiently large F_h ($F_h \sim 1$), two-dimensional flows can be described by Long's model (Long 1953) in which the governing nonlinear equations reduce to a single linear ordinary differential equation when $\rho U^2/2$ and N are independent of height upstream. Solutions of Long's model, valid for steady-state flows in which all streamlines originate upstream (i.e. there are no closed streamlines) show the existence of a gravity-wave field to the lee of the orography. As F_h decreases a critical value is reached (dependent on the orography shape) at which the streamlines begin to overturn (Huppert & Miles 1969) and locally the fluid becomes statically unstable. This 'wave breaking' process is generic to severe downslope windstorms and occurs in both two-dimensional (e.g. Peltier & Clark 1979) and three-dimensional flows (Castro & Snyder 1993) and recent advances in understanding how these windstorms evolve have been made by considering finite-amplitude wave-activity diagnostics in two-dimensional numerical simulations (Scinocca & Peltier 1994).

In this paper we shall attempt to address some of the remaining open questions regarding strongly stratified flows past orography. To this end we present the results of a series of stratified towing-tank experiments conducted at the Environmental Flow Research Centre (EnFlo), University of Surrey. The experiments were designed to answer the following specific questions:

(i) How does the drag vary with F_h for three-dimensional axisymmetric orography in strongly-stratified flows?

(ii) Which processes are responsible for the drag?

(iii) How well do theoretical ideas describe the flows?

(iv) Can gravity-wave motion within a verge region make a significant contribution to the drag?

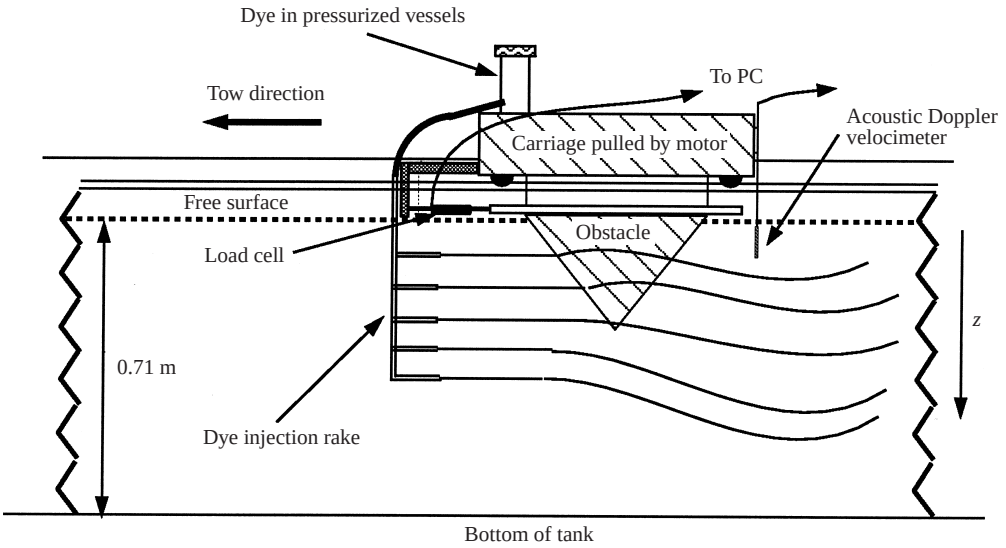

FIGURE 1. Schematic diagram illustrating the EnFlo towing tank apparatus.

The experimental facility is described in § 2 and the results from the drag measurement experiments are presented in § 3. In § 4 specific experiments using dye-visualization and acoustic Doppler velocimeter techniques are described. These were designed to investigate the flow in the summit region (gravity-wave amplitudes and dividing-streamline height) and the middle region (the flow around the obstacles and the flow in the wake). In § 5 some additional drag measurements are made in order to ascertain the importance of vortex shedding and to investigate the effects of a verge region. The results are summarized and conclusions are drawn in § 6.

2. Experimental techniques

The EnFlo stratified towing tank is 12 m long, 1.25 m wide and 1 m deep. Stratification is achieved by filling the tank from the bottom with a mixture of brine and water whose density continuously increases as the tank is filled. A computer-controlled mixing valve allows any specified density profile to be obtained which, in the case of a linear profile, gives a constant value of the buoyancy frequency N with depth, where $N^2 = g/\rho_m \times \mathrm{d}\rho/\mathrm{d}z$, $\rho(z)$ and ρ_m are the density and mean density of the brine–water mixture and z is the vertical coordinate measured downwards from the free surface (see figure 1). The density profiles were measured immediately after the tank was filled using a hand-held density meter; these measurements revealed a very linear density profile. For the drag measurement experiments, typical values of N achieved were between 1.1 and 1.4 s^{-1} and in vortex-shedding experiments, N ranged from 0.45 to 1.6 s^{-1}.

For the drag measurements the obstacles were towed through the tank using methods similar to those of previous experimenters (Castro *et al.* 1990). Briefly, the obstacles were mounted upside down on a stainless steel frame (drag balance) which was suspended (in such a way as to restrict spanwise movement) beneath a carriage that runs smoothly along rails on the top of the tank. The carriage itself was pulled at a constant velocity by an electric motor and each tow commenced with an impulsive start-up of the motor. This start-up procedure generated surface waves, but these were

of very small amplitude and were therefore most unlikely to have had a significant effect on the overall flow field. The tank was filled to give a fluid depth of 0.71 m, leaving 0.5 cm of the obstacles protruding above the free surface. This was necessary to avoid immersing the drag balance itself in the fluid, which would disturb the flow and contribute to the overall drag. Two different capacity load cells (50 N and 10 N) were used to measure the drag exerted on the obstacles during the tows. The load cells were attached between the front of the drag balance and a metal column on the front of the carriage. The arrangement of the whole drag-measurement system is such that only the streamwise component can be measured. A schematic diagram of this apparatus is presented in figure 1. Flow visualization was achieved using a dye-injection technique. A food dye–water mixture, of the same density as the fluid in the tank at the depth of injection, was injected (at up to five levels simultaneously) from a rake upstream of the obstacle on the spanwise centreplane. The injection rate was controlled so that velocity of the dye was the same as the tow speed. Video cameras were positioned on mountings attached to the side of the carriage and on a separate carriage below the tank which was pulled along at the tow speed. Measurements of the dye motion were made by analysing the recordings of the tows with frame-grabbing software on a computer and applying appropriate corrections for parallax. Note that these parallax corrections did not allow for the bending of light rays due to changes in the refractive index caused by the stratification. Such effects were investigated by suspending a large flat board (upon which a Cartesian grid was drawn) in the tank and taking still images with the video camera mounted at the side of the tank (which was positioned 985 mm from the spanwise centreplane and typically 300 mm below the level of the free surface). The grid was suspended in a vertical plane a range of distances (up to 200 mm) from the centreplane and images of the grid were compared under conditions of neutral stratification and linear stratification. Changes in the positions of specific points in the images caused by the stratification were found to be negligible, indicating that these refractive index effects could be neglected. Velocity measurements were made in the wake of the obstacles using a Nortek Acoustic Doppler Velocimeter. The probe was attached to a track on the rear of the carriage and its position could be adjusted in the vertical and spanwise directions.

The stratification is very robust in the sense that it is quite unaffected by towing obstacles through the tank. In fact, after a complete day's work (which would typically involve 5 tows) the only significant changes in the density profile occurred at the free surface and the bottom of the tank where neutral layers of a few centimetres in depth formed. The lack of change in the density profile over the bulk of the fluid (noted also by previous researchers including Rottman & Britter 1986) is primarily due to the strong stratification which inhibits vertical mixing and the fact that, compared to the kinematic viscosity of the fluid ($\approx 10^{-6}\,\mathrm{m^2\,s^{-1}}$), the coefficient of diffusivity of salt in water is small ($\approx 1.5\times10^{-9}\,\mathrm{m^2\,s^{-1}}$). Due to the slow erosion of the density profile at the bottom and immediately under the free surface, the tank was re-filled every morning before experiments began. For some of the later vortex-shedding measurements even greater control of the linearity of the density profile near the surface was achieved by frequent use of a 'skimmer' to remove the top few centimetres of fluid (while re-filling from the bottom to maintain a constant depth).

Experiments were conducted under both stratified and neutral conditions for a variety of obstacle shapes and sizes. In order to investigate the dependence of drag, gravity-wave generation, wake structure and dividing-streamline height on obstacle shape, two basic shapes were chosen. These were a hemisphere (which has a smooth,

flat summit) and a cone (which has a pointed summit). The hemispheres allow some comparison with previous results since some earlier work has focused on flat-topped obstacles (e.g. Hunt & Snyder 1980). The cones, on the other hand, are a more realistic representation of steep mountain summits, although admittedly they are somewhat steeper than the mountain tops that occur in nature. In order to examine the effect of blockage due to the finite width and height of the tank, two sizes of hemisphere were used, with base radii of 200 mm and 150 mm. We shall refer to these hemispheres as HS1 and HS2, respectively. Two shapes of cone were chosen. These both had the same height, 250 mm, but different radii of 250 mm and 100 mm, giving slopes of 1 and 2.5. We shall refer to these as cones C1 and C2, respectively.

3. Drag measurements on the cones and hemispheres

3.1. *Results for neutral flow*

One of the main problems associated with the applicability of towing-tank experiments to the atmospheric scale is that viscous effects at laboratory scales will undoubtedly be different from those in the atmosphere. Typical Reynolds numbers for orographic flows modelled in the towing tank, $Re = UL/\nu$, where L is the obstacle base width and ν is the kinematic viscosity are $\sim 10^4$ whilst for atmospheric flows they are $\sim 10^9$. This huge difference means that before laboratory results can be applied to the atmosphere we must investigate and to some extent remove any Reynolds number effects. With this in mind the drag was measured on the cones and hemispheres under neutral conditions (and thus without the additional complicating effects of stratification) for a variety of different carriage speeds. For each tow the load-cell signal was sampled at a frequency of 100 Hz. An example of the drag signal obtained from the 50 N load cell is given in figure 2(*a*). After some initial large-amplitude high-frequency oscillations in the drag (due to the impulsive start-up of the carriage), the measured drag appears to settle down to a quasi-steady state until the endwall is approached after about 90 s. For each tow a mean drag coefficient was calculated, defined by

$$C_d = \frac{\overline{\tau}}{\frac{1}{2}\rho U^2 A}, \tag{3.1}$$

where $\overline{\tau}$ is the average drag calculated over periods when the drag remained approximately steady and A is the frontal cross-sectional area of the obstacle. Each tow was repeated at least three times. Errors associated with the zero offset of the load cells meant that for the lowest tow speeds (for which the measured drag is smallest) the C_d results were only repeatable to within $\sim 10\%$. At higher speeds the repeatability was much better. Figure 2(*b*) shows the variation of the drag coefficient with Re for the four obstacles. These drag coefficients are calculated from the average value of C_d (based on at least three tows) at each Re. To aid interpretation, smooth curves have been drawn through the drag coefficient data. Typical error bars, based on a pessimistic estimate of 10% accuracy, have been added to this and all following drag plots.

The drag coefficients, caused by flow separation and skin friction, are somewhat Reynolds number dependent for the lower values although the curves do appear to level off for $Re \gtrsim 5 \times 10^4$. The Reynolds number dependence reveals the importance of viscous effects on the flow despite the relatively large scale of the obstacles used in this study compared to some previous work (e.g. Brighton 1978). This must be taken into account when interpreting the results in the stratified case and we shall attempt

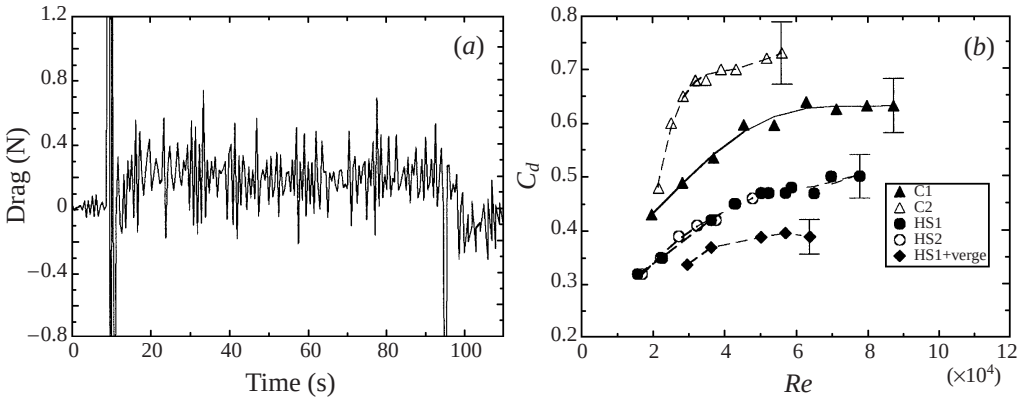

FIGURE 2. (*a*) The evolution of the drag (after smoothing) during a tow of the hemisphere HS1 under neutral conditions at a speed of 10.8 cm s^{-1} ($Re = 4.3 \times 10^4$) and (*b*) the drag coefficient, C_d, vs. Re for the four obstacles C1, C2, HS1 and HS2 under neutral conditions. Also included are drag coefficient measurements on the hemisphere HS1 with attached verge region which are described in detail in § 5.

this by normalizing the stratified drag measurements by the drag in neutral flow at the same Reynolds number. Note that the drag data for the two hemispheres collapse onto the same curve, indicating that any blockage effects (due to the presence of the tank sidewalls and floor) are minimal for neutral stratification.

3.2. *Results for stratified flow*

The tows were repeated in the stratified case and variation in F_h was achieved by altering the tow speed rather than the density profile. The variation of the drag coefficient in the stratified case, C_{ds}, with F_h is shown in figure 3. Figure 4 shows the variation of the ratio of the stratified drag to the neutral drag at the same Reynolds number, C_{ds}/C_d, with F_h. To aid interpretation cubic splines have been fitted through the data. Both C_{ds} and C_{ds}/C_d generally increase with decreasing F_h for all four obstacles. The stratification appears to significantly increase the drag for $F_h \lesssim 0.4$ for all the obstacles and the maximum measured values of C_{ds}/C_d are 3.9, 2.8, 5.4 and 2.9 for C1, C2, HS1 and HS2, respectively. Note that although the drag coefficients are highest for the low values of F_h, the actual drag exerted on the obstacles is very small, meaning that the repeatability of these experiments is poorer than at the higher values of F_h and we were unable to obtain reliable data for values of $F_h \lesssim 0.15$. Note also that the data for the two hemispheres do not collapse onto the same curve and that the differences are largest for low values of F_h. We shall return to this point in § 5.1.

Lofquist & Purtell (1984) have presented drag results for a sphere at lower Reynolds numbers than those studied here. The sphere, radius r, was submerged in the centre of a stratified towing tank. For values of their stratification parameter $\kappa = Nr/U < 3.5$ (κ is equivalent to F_h^{-1} in our experiments) their measurements reveal a trend for $\Delta C_d = C_{ds} - C_d$ to decrease with decreasing κ. This is equivalent to the general trend that we see (i.e. C_{ds}/C_d decreasing as F_h increases). However, Lofquist & Purtell's data show a large maximum in ΔC_d at $\kappa = 3.5$ ($F_h = 0.29$) and for more strongly stratified flows the drag coefficient decreases (see their figure 4). A similar maximum in the drag coefficient is also found by Mason (1977) (see his figure 6). Although we are unable to obtain reliable drag measurements when $F_h \lesssim 0.15$ it is clear from our data that

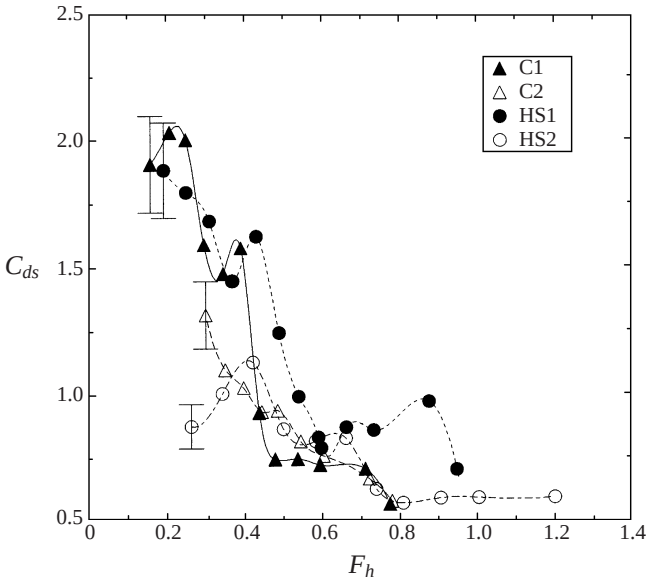

FIGURE 3. The variation of the drag coefficient, C_{ds}, with F_h for the four obstacles under stratified conditions.

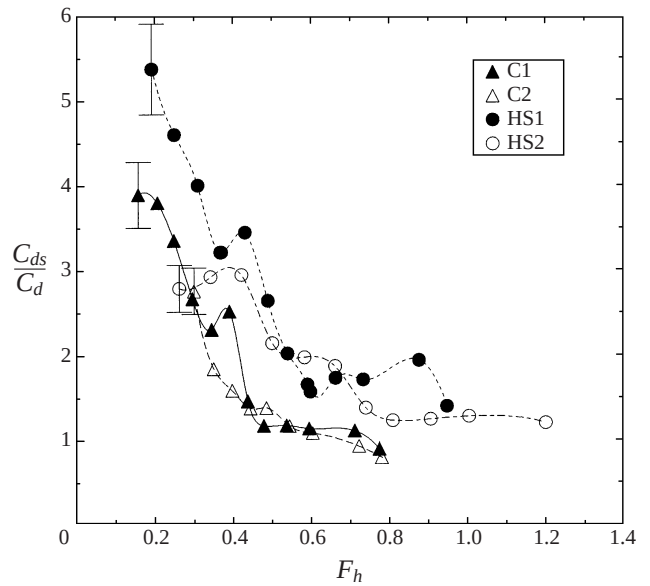

FIGURE 4. The variation of the ratio of drag coefficients, C_{ds}/C_d, with F_h for the four obstacles.

if such a maximum does exist, it occurs at a much lower Froude number than that found by Lofquist & Purtell (1984) and Mason (1977). Local maxima and minima in the drag coefficients do occur though and it seems that these are due to the finite depth of the tank. As demonstrated by Castro *et al.* (1990), minima in the drag occur for integer values of the parameter $K = ND/\pi U$. Figure 5, showing C_{ds}/C_d vs. K for the hemisphere HS1, reveals that this is true in our experiments also; minima occur

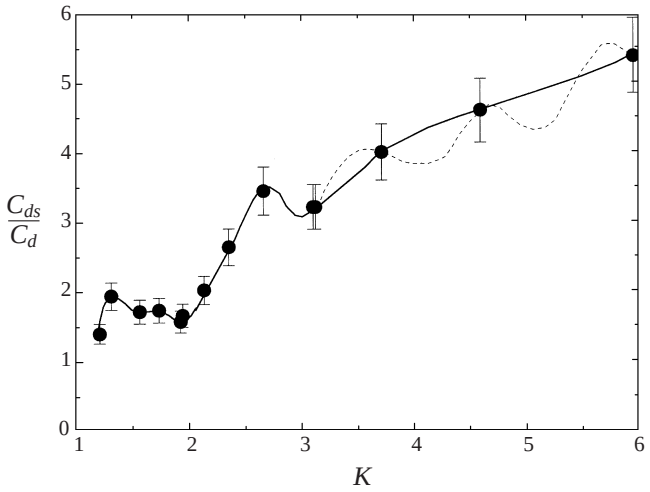

FIGURE 5. The variation of the ratio of drag coefficients, C_{ds}/C_d, with K for the hemisphere HS1. The dashed curve shown for $K > 3$ is speculative.

near $K = 2$ and $K = 3$. We can only speculate that this behaviour continues above $K = 3$ since we do not have enough data in this range. However, we might expect the size of the variations in C_{ds}/C_d to decrease as K increases, since the amplitude of the gravity-wave motions decreases (see § 4.1).

4. Flow visualization and velocity measurements

4.1. *Gravity-wave measurements*

Measurements of gravity-wave amplitudes were made by releasing dye upstream of the obstacles between heights of h and $1.45h$. Snapshots were obtained from video footage of the tows and the amplitude of the wave motion in the lee of the obstacles was measured using the computer-based image analysis system. An example of such a snapshot is given in figure 6(a) which shows the flow over the hemisphere HS1 when $F_h = 0.33$. In this particular case the waves in the lee of the obstacle are almost overturning. Indeed, soon after this instant a turbulent patch developed where the waves began to break. Figure 7(a) shows the peak-to-peak vertical displacement in the lee of the obstacle along the path of dye which was released upstream at the summit height (an example of this is marked in the schematic diagram in figure 6(b)). Cubic splines have been fitted through the data to aid interpretation. The wave amplitude appears to be $O(F_h h)$ for all the obstacles, although for $F_h \gtrsim 0.3$ the waves generated by the narrow, steep cone C2 are significantly smaller than those generated by the other shapes. The general trend is clearly one of increasing wave amplitude with increasing F_h. Figure 7(b) shows the peak-to-peak amplitude normalized by r, where r is the obstacle radius at the base. This choice of normalization (whose effect on figure 7(a) is to change the C2 data only since $h/r = 1$ for all the other obstacles) improves the collapse of the data somewhat since the amplitudes for the two cones are now similar. Figure 8(a) shows the wave amplitude (normalized by h) when the dye is released at $1.35h$. Again, there is a general trend for the amplitudes to increase with F_h and the amplitude is substantially smaller for the cone C2. Normalising these wave amplitudes by r again improves the collapse of the data (see figure 8b)

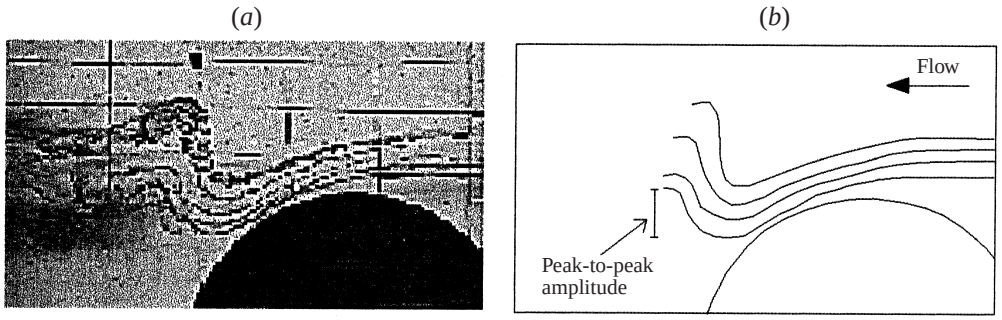

FIGURE 6. Visualization of wave generation by the hemisphere HS1 when $F_h = 0.33$ from (*a*) video footage and (*b*) a schematic illustration of the flow. The flow, relative to the obstacle, is from right to left in both pictures. Also marked in (*b*) is the peak-to-peak amplitude of the vertical displacement of the dye released at summit height.

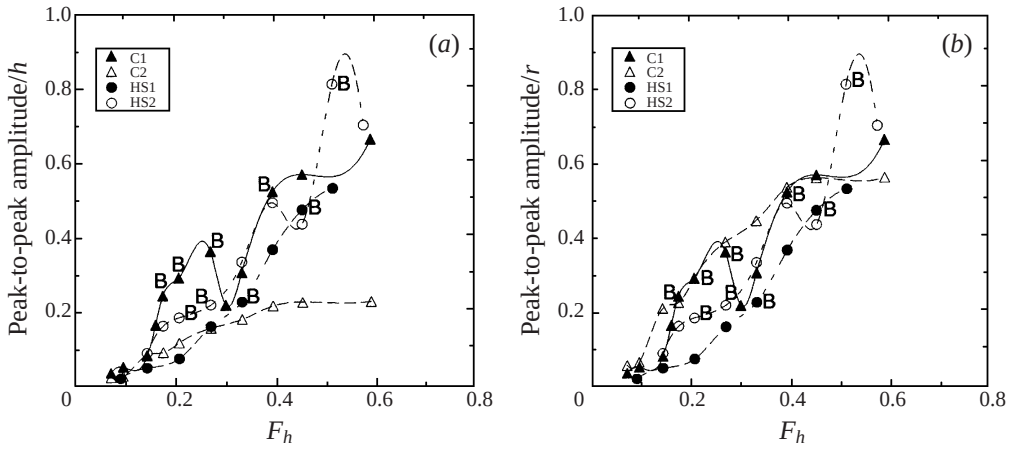

FIGURE 7. The wave amplitude determined from the peak-to-peak displacements of dye released at the summit height (*a*) normalized by h and (*b*) normalized by the radius r. The letter 'B' denotes wave breaking.

indicating that for the cones, the slope may play an important role in determining the wave amplitude. The fact that the waves generated by C2 are of small amplitude compared to those generated by C1 is consistent with the idea that as the radius reduces to zero (a 'needle' shape) one intuitively expects small amplitudes. This is easily explained by considering the spectrum of wave modes forced by these shapes. Linear theory indicates that a given stationary mode, with horizontal wavelength λ, exists only if $\lambda \geqslant 2\pi F_h h$ and will decay exponentially in the vertical otherwise. Clearly the spectrum of the steeper cone is such that short-wavelength modes are forced in preference to longer wavelengths and, since as F_h increases the minimum permissible wavelength increases, we would expect the waves forced by the cone C2 to be of smaller amplitude than those forced by C1.

Wave breaking was observed in the lee of obstacles C1, HS1 and HS2 at certain values of F_h and these are marked on figures 7 and 8 with the letter 'B'. Note that, consistent with the fact that the waves generated by the cone C2 were significantly smaller than those generated by the other obstacles, no wave breaking was observed for this obstacle. The wave breaking was not always a steady phenomenon: at

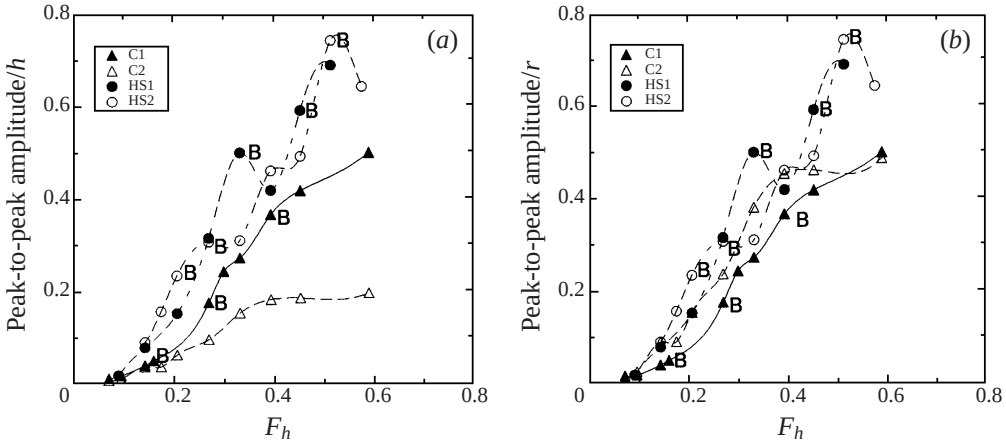

FIGURE 8. The wave amplitude determined from the peak-to-peak displacements of dye released at $1.35h$ (*a*) normalized by h and (*b*) normalized by the radius r. The letter 'B' denotes wave breaking.

$F_h = 0.45$ the breaking in the lee of hemisphere HS1 occurred at the start of the tow and had ceased by the halfway point of the tow and at $F_h = 0.51$ (hemisphere HS2) and $F_h = 0.27$ and 0.39 (cone C1) the breaking occurred towards the end of the tows. In the latter three cases it seems possible that the breaking was influenced by endwall effects, e.g. reflection of upstream propagating modes. Apart from these transient cases the breaking appears to be restricted to a fairly narrow interval in F_h ($0.16 \leqslant F_h \leqslant 0.32$). This is consistent with results obtained by Castro & Snyder (1993) who examined the wave-breaking regimes for a variety of hill shapes over a range of spanwise aspect ratios and found that there existed upper and lower critical values of F_h between which wave breaking occurred. The suppression of wave breaking at very low values of F_h should perhaps be expected since the wave amplitude is very small. Despite the fact that it is not strictly valid for this flow regime, the disappearance of wave breaking at the higher values of F_h can be predicted, at least qualitatively, by linear theory (Smith 1989). The physical reason for the disappearance of the wave breaking is simply that, due to the increase of the horizontal wavelength as F_h increases, the waves (whose amplitudes are determined by, amongst other things, the Fourier decomposition of the obstacle shape) become de-tuned to the shape of the obstacle.

As discussed by Hunt & Snyder (1980), for hills with small slope, under weakly stratified conditions ($F_h \gg 1$), the occurrence of flow separation on the downwind slope of the hill will be controlled by boundary-layer processes. At smaller Froude numbers ($F_h \sim 1$), however, separation can be controlled by the pressure distribution produced by the gravity-wave train. Further, if the wavelength of the gravity waves is similar to the characteristic width of the hill then flow separation may be completely suppressed as the waves become 'tuned' to the hill shape. Hunt & Snyder's (1980) experiments indicated that this could occur for both two-dimensional and three-dimensional axisymmetric hills. Under these circumstances, there will presumably be a corresponding increase in the drag and wave amplitude. For hills of small slope, when the depth of the fluid, D, is large compared to the hill width, L, linear theory indicates that the horizontal wavelength of the gravity-wave train is $\approx 2\pi F_h h$. We would therefore expect flow separation to be suppressed and the waves to be tuned to the hill shape at the critical Froude number, $F_{h_{\text{crit}}} = L/2\pi h$. In the present study, flow

visualization reveals that flow separation occurs over the whole range of F_h examined ($0.07 \leqslant F_h \leqslant 0.59$) and the waves do not appear to become tuned to the obstacle shape. An example of the flow separation can be seen in figure 6. Presumably, the reason for the separation is simply the fact that the obstacles all have steep slopes and thus the critical Froude numbers are considerably smaller than unity ($F_{h_{\text{crit}}} = 1/\pi$ for the hemispheres and cone C1 and $F_{h_{\text{crit}}} = 2/5\pi$ for the cone C2). At such small Froude numbers, since the bulk of the flow is around rather than over the orography (see § 4.2), the waves are of insufficient amplitude to prohibit flow separation.

The fact that the wave amplitude generally increases whilst the drag coefficient decreases with increasing F_h is contrary to what occurs at much higher values of F_h, where (as correctly indicated by linear theory) the wave amplitude and drag coefficient are linked and both increase as F_h decreases from infinity. At lower values of F_h ($F_h \gtrsim 1$), inviscid linear theory for flow past three-dimensional orography (e.g. Smith 1988) indicates that the pressure perturbation on the surface of the obstacle is $O(\rho U^2 F_h^{-1})$ and thus $C_{ds} \propto F_h^{-1}$. Since in this regime fluid parcels which originate at $z = 0$ upstream are able to travel over the summit, the wave amplitude is $O(h)$. Although the behaviour of the drag coefficient would appear consistent with our measurements, the wave amplitude is clearly not. In order to allow for the fact that when $F_h \lesssim 1$ some of the flow passes around the obstacle rather than over the summit we might consider a Drazin-like solution in the middle region, which makes no contribution to the drag, and apply the linear solution to the summit region only. This effectively reduces the height of the orography to $O(F_h h)$ and thus the wave amplitude will now be $O(F_h h)$ also. Accounting for the decrease in frontal cross-sectional area on which the force is exerted, such an approach gives rise to a drag coefficient $\propto F_h^2$. Despite the fact that this conceptual model provides a better representation of the flow than the more conventional application of linear theory and that the wave amplitude is now consistent with that seen in the experiments, the predicted variation of the drag coefficient is clearly very different. It is clear that the observed drag is not easily explained by gravity-wave generation alone and we shall return to this point in § 5.

4.2. *Dividing-streamline height measurements*

Attempts to measure the dividing-streamline heights for the four obstacles were made by releasing dye close to the summits of the obstacles and, based on video footage, deciding whether or not the dye passed over the summit of the obstacles or travelled around the sides. These measurements were complicated by unsteadiness present in the flow immediately upstream of the obstacles. Dye released on the obstacles' centreplanes switched periodically from flowing around one side of the obstacle to the other. It was therefore necessary to base the measurements on snapshots of the flow taken at times when the dye was impinging on the centreplanes of the obstacles. The measurements were repeated for a range of F_h and the results are illustrated in figure 9. Also shown is Sheppard's formula, equation (1.1). For both sizes of hemisphere equation (1.1) provides a good estimate of the dividing-streamline height. For the cones, however, it appears to underestimate it. The reason for this is not entirely obvious and these results need to be interpreted with a degree of caution. In neutral flow one would expect all streamlines on an obstacle's centreplane to pass over the summit, regardless of the shape of the obstacle. Even when the flow is stably stratified the fluid parcels possess enough kinetic energy to travel over the top. Certainly, the unsteadiness present in the flow makes these measurements quite difficult and it is hard to estimate the errors involved. Indeed, for the cones, whose

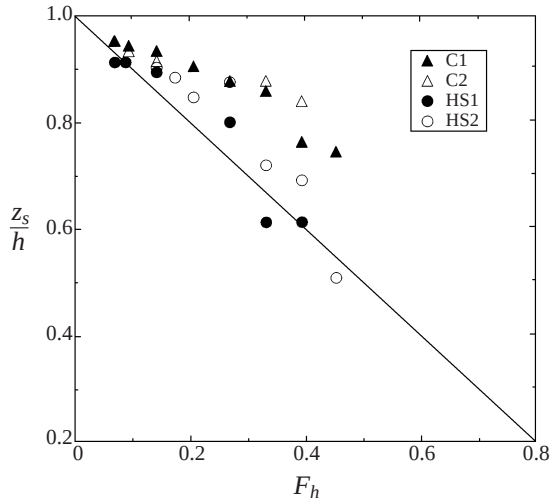

FIGURE 9. Dividing-streamline heights deduced from dye released upstream of the hemispheres and cones. Also shown is the estimate given by Sheppard's formula, equation (1.1).

summits are narrow in comparison to the hemispheres, the unsteadiness makes the timing of the measurements critical. Another complicating factor is that due to the spanwise oscillatory motion in the approaching flow (induced by vortex shedding in the wake), the dye has a non-zero spanwise component of velocity as it travels towards the summit of the obstacle. This may cause a tendency for the dye to travel over the shoulder of the obstacle rather than directly over the summit. Such an effect would be more important for obstacles with narrow summits (e.g. cones) than for flat-topped shapes. Despite these reservations, figure 9 indicates that for all four obstacles, Sheppard's formula at least provides a necessary condition for fluid parcels to travel over the summits, if not a sufficient one.

4.3. *Measurements of the flow around the obstacles*

The inviscid steady-state ideas of Drazin (1961) indicate that for small F_h, away from the summit of the obstacle, the flow around the obstacle should be essentially two-dimensional with vertical deflections limited to $O(F_h^2 h)$. In order to test the relevance of these ideas to the tank experiments, dye was released upstream of the obstacles at heights between $0.54h$ and $0.65h$ and measurements were made of δ, defined as the maximum vertical deflection of the dye from its upstream height as it passes around the obstacle. The deflection of the dye was always downwards (i.e. towards the base of the obstacle) and this is illustrated by the example provided in figure 10(a) which shows a side view of the flow around the hemisphere HS2 when $F_h = 0.27$. There are two difficulties associated with making such measurements. First, the spanwise unsteadiness (see § 4.2) means that the measurements can only be made as the dye crosses the centreplanes of the obstacles. Secondly, as F_h increases the position of the maximum vertical displacement shifts further downstream of the obstacle. For the higher values of F_h this position is located in a turbulent wake, making the measurements very difficult. This was a serious problem with the cone C2 for which reliable data could only be obtained for $F_h < 0.15$. Figure 11 shows the variation of δ with F_h. It appears that for all four obstacle shapes δ increases with increasing F_h. It is, however, difficult to draw any conclusions regarding the exact dependence on F_h:

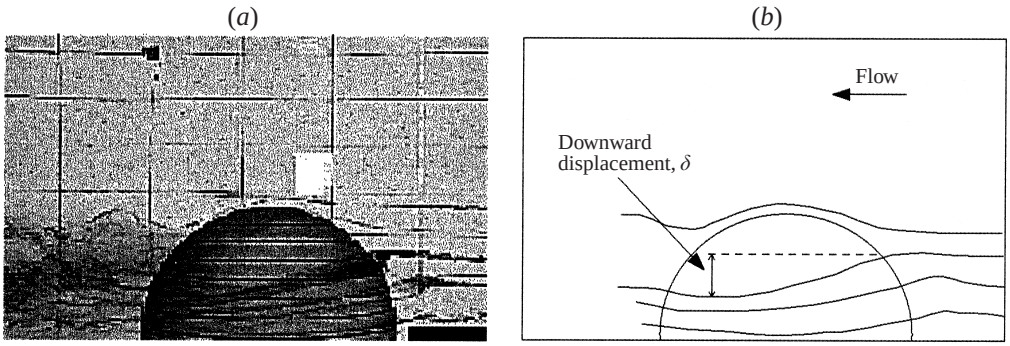

FIGURE 10. Visualization of the flow past the hemisphere HS2 when $F_h = 0.27$ from (*a*) video footage obtained from the side of the tank as the dye crosses the centreplane of the obstacle and (*b*) a schematic illustration of the flow. The flow is from right to left relative to the obstacle in both pictures. Also marked in (*b*) is the maximum downward deflection of the dye, δ.

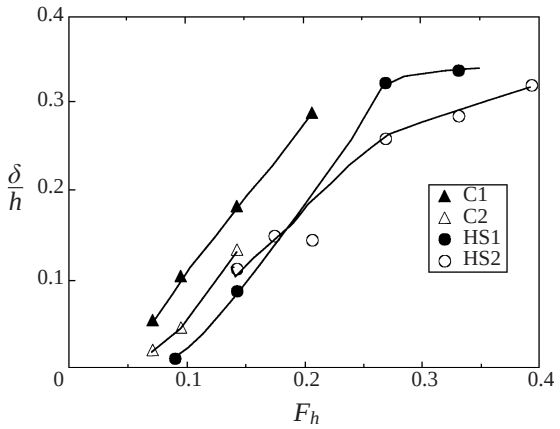

FIGURE 11. The maximum downward deflection of dye, δ, from its upstream level. The dye was released at heights of $0.54h$, $0.54h$, $0.55h$ and $0.65h$ upstream of the obstacles C1, C2, HS1 and HS2, respectively.

δ/h appears to vary linearly with F_h although such a dependence would also suggest a non-zero intercept on the F_h-axis, which is hard to justify physically. It appears that further measurements of δ, at values of F_h lower than those studied here, would be needed to draw any firm conclusions regarding the validity of Drazin's theory.

4.4. *Measurements in the wake*

Releasing dye upstream between the summits and bases of the cones and hemispheres revealed the presence of an unsteady wake in which vortex shedding occurs. The flow could be seen to separate from the sides of the obstacles, though the positions of the separation points were unsteady and dependent on height, and vortices were shed in the wake periodically. Consistent with the findings of Brighton (1978), the dye motion suggests that the period of the vortex shedding does not vary with height. Obtaining reliable measurements of the shedding period over a range of F_h and Re using dye visualization alone proved to be very difficult, due mainly to the turbulent nature of the wake at the higher Reynolds numbers. Instead, an alternative technique, using a Nortek Acoustic Doppler Velocimeter (ADV) to make continuous measurements of

the velocity in the wake was employed. The ADV is of the 5 cm downward-looking three-dimensional variety and further details of it can be found in Snyder & Castro (1998). The probe was positioned 0.8 $\pm$0.1 m downstream of the obstacle centres and its lateral position was typically a distance $0.5L$ to L off the centreline, where L is the obstacle base width. For the vast majority of tows the height at which the measurements were made (5 cm below the probe itself) was adjusted to $h(1-F_h)/2$. Assuming the dividing-streamline height, z_s, is given by formula (1.1), then this is equal to $z_s/2$. During each tow the velocity in the wake was sampled at 25 Hz and traces of both horizontal velocity components were found to be quite periodic. The vertical velocities were generally negligible in this region. A typical horizontal velocity trace, taken for the cone C2 when F_h =0.1, is shown in figure 12. Velocity measurements were made for values of F_h between 0.05 and 0.4 and the horizontal components showed periodic oscillations over this range, indicating the occurrence of vortex shedding. Note that periodic shedding was sometimes absent at $F_h = 0.3$ for the cone C2 and so no tows were performed at higher Froude numbers for this obstacle. Shedding frequently disappeared at $F_h = 0.4$ for the other obstacles and for this reason, and the fact that for the smaller obstacles positioning the probe to measure at half the dividing-streamline height became increasingly difficult, no ADV measurements were made for $F_h > 0.4$. Note that the persistence of vortex shedding for Froude numbers as high as 0.4 is contrary to the results from Brighton's (1978) experiments, for which the shedding disappeared above $F_h = 0.15$, but is consistent with results from other towing-tank studies, e.g. the experiments of Castro *et al.* (1983) in which shedding occurred at $F_h = 0.3$ but not at 0.4. Our results are also similar to those from numerical simulations. Paisley & Castro (1995) conducted high Reynolds number simulations of stratified flows past bell-shaped mountains and found that vortex shedding occurred below $F_h = 0.2$ but at $F_h = 0.3$ the wake remained steady. The reason for the disappearance of the shedding in Brighton's (1978) experiments at such a low Froude number is unclear, but is perhaps a Reynolds number effect, since his experiments were conducted at considerably smaller Re. It is also interesting to make comparisons with towing-tank studies of wakes behind spheres in stratified flows. Chomaz, Bonneton & Hopfinger (1993) found that two-dimensional vortex shedding occurred behind spheres when $F_h \lesssim 0.5$ and that at even higher values of F_h ($0.5 \lesssim F_h \lesssim 0.7$), although the two vortices behind the sphere did not actually separate, the wake was still unsteady due to a periodic oscillation in the position of the two vortices. These findings are somewhat different to our results for the hemispheres and cones.

In almost all cases the shedding frequencies were computed from both the horizontal velocity traces separately by calculating an average period for each trace. Typically, these values differed by less than 3%. For each tow an average value, based on the values obtained from the two traces, was then calculated. A few additional tows were repeated with the probe positioned at different heights. These revealed no significant change in the period of the velocity signals, although the amplitude did vary and shedding was not discernible for $z \gtrsim z_s$ (again assuming $z_s/h = 1-F_h$). The difficulty with calculating a non-dimensional shedding frequency, or Strouhal number, for these flows is that unlike the case of a two-dimensional obstacle (e.g. a cylinder or rectangular plate) where the relevant length scale is simply the obstacle diameter, when the diameter of the obstacle varies with height it is not clear what length scale is appropriate. The simplest idea is to use the base width of the obstacles and define a Strouhal number, $S = fL/U$ where f is the frequency of the vortex shedding measured from the velocity traces. Figure 13(a) shows how S depends on F_h for the

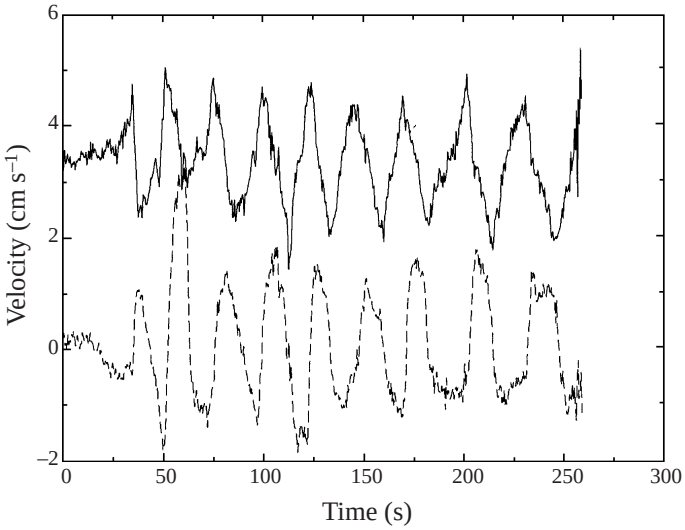

FIGURE 12. ADV measurements of streamwise (solid line) and spanwise (dashed line) velocity made during a tow of the cone C2 when $F_h = 0.1$, $Re = 6750$. The probe was positioned $4.07L$ downstream of the centre of the cone and $0.9L$ from the centreline.

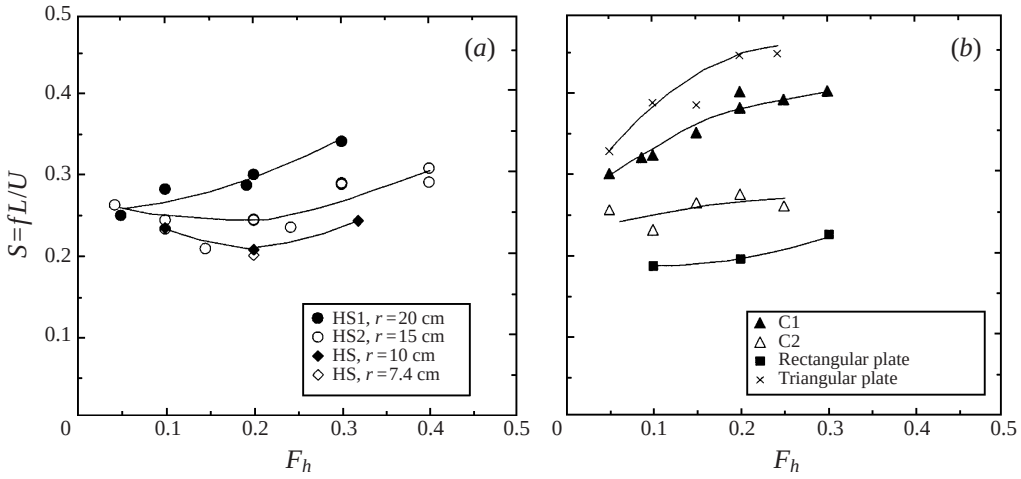

FIGURE 13. The variation of the Strouhal number, $S = fL/U$, with F_h for (*a*) the hemispheres and (*b*) the cones and triangular and rectangular plates.

hemispheres HS1 and HS2. Note that results from some tows of smaller hemispheres with radii of 100 mm and 74 mm are also presented. Strouhal numbers for the cones C1 and C2 are presented in figure 13(*b*). Also shown are Strouhal numbers for two different shapes of flat plate although we defer discussion of these latter results. For both the cones and hemispheres, there appears to be a slow increase of S with increasing F_h and the values of S are clearly quite different for the different shapes and even different sizes of the same shape (figure 13*a*).

It seems reasonable to suppose that the width of the wake might be determined by the width of the obstacles at some height below the dividing-streamline height. Based on this hypothesis, one possible relevant length scale is L_2, the diameter of the

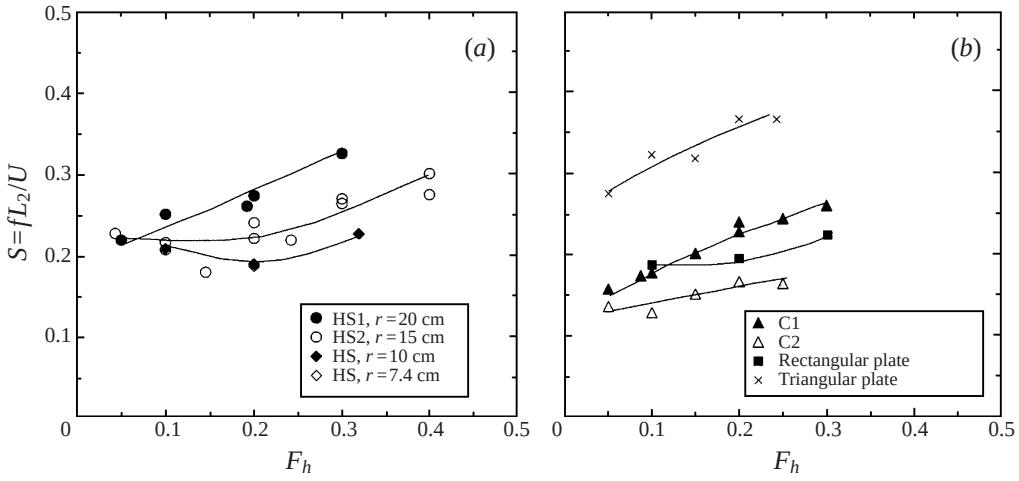

FIGURE 14. The variation of the Strouhal number, $S_2 = fL_2/U$, with F_h for (*a*) the hemispheres and (*b*) the cones and triangular and rectangular plates.

obstacle at half the dividing-streamline height, where once again we shall assume that z_s is given by equation (1.1). Figure 14(*a*) shows the variation of the Strouhal number, $S_2 = fL_2/U$, with F_h for the hemispheres. Similarly, Strouhal numbers for the cones C1 and C2 are presented in figure 14(*b*). Figures 13(*a*) and 14(*a*) indicate that, as for the drag coefficient measurements, the Strouhal numbers for the hemispheres do not collapse onto the same curve. In fact there is a general trend for the Strouhal number to fall as the size of hemisphere decreases. This effect is clearly due to either Reynolds number or blockage differences. Unlike the neutral flow case, when $F_h \ll 1$ one might expect blockage effects to be more significant because the flow is largely constrained to move in two-dimensional planes. We have attempted to correct for blockage effects by considering the average speed through the vertical plane which intersects the obstacle centre and is orientated spanwise across the tank. For an obstacle whose width is independent of height, if the flow is two-dimensional, then to first order this average speed is $U/(1-L/W)$, where W is the width of the tank, since the mass flux at the side of the obstacle must equal that upstream. In the present study the situation is complicated by the fact that the widths of the obstacles vary with height and therefore we shall define a blockage-corrected speed as

$$U_c = \frac{U}{1 - L_2/W}. \tag{4.1}$$

We can now attempt to correct for blockage effects by defining a corrected Strouhal number $S_{2_c} = fL_2/U_c$. Figures 15(*a*) and 15(*b*) show how S_{2_c} varies with the effective Froude number, $F_{h_c} = U_c/Nh$, for the hemispheres and the cones, respectively. The collapse of the data for all sizes of hemisphere appears to have improved considerably (cf. figure 14), indicating that blockage effects are important in these flows. The collapse of the cone data is also significantly improved. Comparing 15(*a*) and 15(*b*) shows that the values of S_c for the cones are themselves similar (albeit slightly smaller) to those for the hemispheres although, of course, there is no *a priori* reason why we would expect the cone data to collapse onto the hemisphere data, especially considering that as F_h increases the flow becomes increasingly three-dimensional.

Note that one might prefer, in principle, to use a correction known to be more

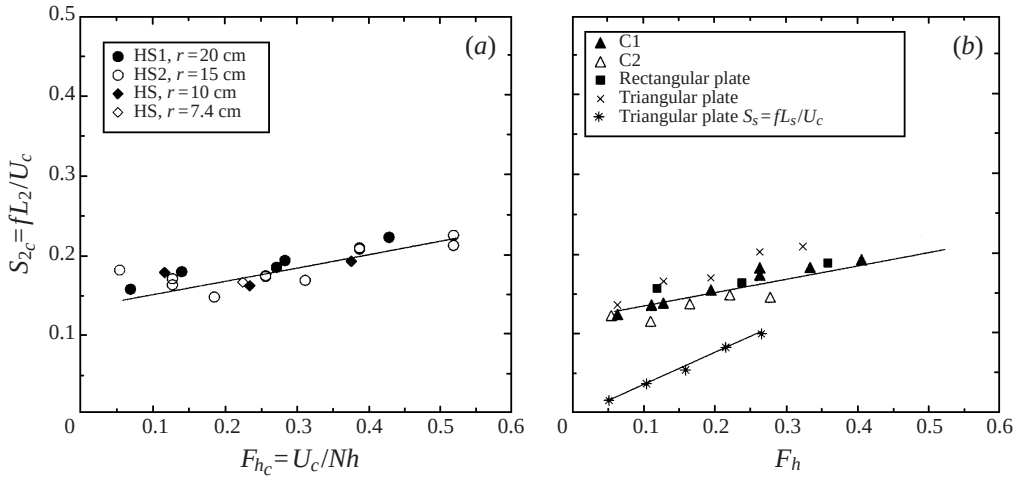

FIGURE 15. The variation of the Strouhal number, $S_{2_c} = fL_2/U_c$, corrected for blockage, with the effective Froude number $F_{h_c} = U_c/Nh$ for (*a*) the hemispheres and (*b*) the cones and triangular and rectangular plates. Also shown in (*b*) is the Strouhal number, $S_s = fL_s/U_c$, for the triangular plate.

soundly based for bluff bodies rather than the correction used here. However, we found that a correction using, for example, Maskell's (1965) theory (a semi-empirical correction for neutral flow past bluff bodies which is based on an approximate relation for momentum balance in the flow outside the wake) did not improve the degree of collapse in Strouhal number above that shown in figures 15(*a*) and 15(*b*) or improve the collapse between the different shaped bodies. If anything, the collapse was made slightly worse.

Reynolds number effects on the Strouhal number measurements have also been investigated by plotting S_{2_c} against Re for fixed values of Froude number. Figure 16, which shows the Reynolds number dependence of the blockage-corrected Strouhal numbers for the hemispheres when F_h is fixed at 0.1 and 0.2, suggests that such effects are quite weak.

It is interesting to compare the Strouhal number results with measurements made in neutral flow. Neutral measurements of S made by Trischka (1980) at $Re = 10^4$ are ~ 0.25 and ~ 0.23 for cones with the same slope as C1 and C2, respectively. These values are somewhat higher than the values of S_{2_c} we see in stratified flow although figure 15(*b*) reveals that for weaker stratification our values for all the obstacles approach those found by Trischka. It is also instructive to compare with measurements made by previous researchers in stratified flows. Towing-tank work at lower Reynolds numbers by Lin *et al.* (1992) and Chomaz *et al.* (1993) indicate Strouhal numbers for spheres of around 0.2. This is of similar magnitude to the values of S_{2_c} for the hemispheres when $F_h \lesssim 0.2$ (see figure 15). Towing-tank experiments conducted by Castro *et al.* (1983) revealed values of S (based on the spanwise width of their three-dimensional triangular ridges) between 0.14 and 0.18 and numerical simulations of stratified flows past bell-shaped orography by Paisley & Castro (1995) predict a Strouhal number of about 0.2. These values are all of a similar magnitude to the measurements of S_{2_c} presented in figure 15 although the usefulness of such a comparison must be questioned since previous authors have not taken blockage effects into account. Brighton's (1978) measurements of the Strouhal number for a hemisphere ($S = 0.44$ when $F_h = 0.084$) is very different from our, and all other,

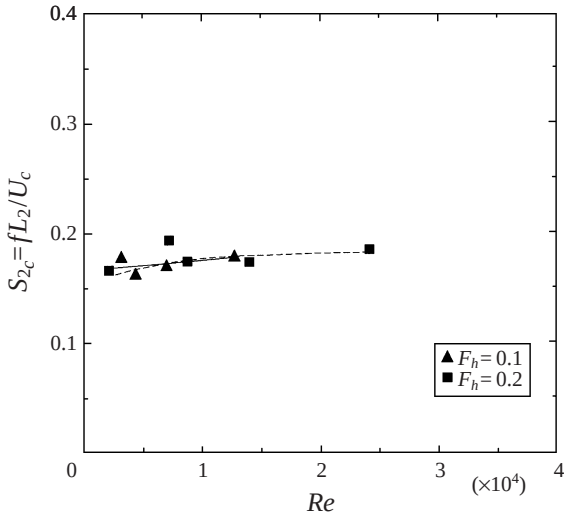

FIGURE 16. The variation of the Strouhal number corrected for blockage, $S_{2_c} = fL_2/U_c$, with Reynolds number for the hemispheres when F_h is fixed at 0.1 and 0.2.

measurements. Presumably this is again due to the low Reynolds numbers at which his experiments were conducted. Finally, it is interesting to compare the Strouhal numbers measured in the laboratory with those estimated from satellite imagery of atmospheric flow past islands. Case studies presented by Berlin (1981) of vortex streets behind the islands of Gran Canaria and La Palma suggest Strouhal numbers (based on the spanwise distance between successive vortices rather than island diameter) in the range 0.21–0.34. Despite the obvious additional complexity of the atmospheric flows due to the complicated orography and variability in the background flow, these values are somewhat similar to the ones obtained in the laboratory. Recently, Smith, Gleason & Gluhosky (1997) have used satellite imagery to observe the wakes behind islands in the Caribbean. However, comparison between their observations and the laboratory experiments is not possible since they studied 'weak' wakes only, in which the vorticity is not strong enough to form eddies but is instead advected downstream.

As mentioned previously, both the dye-injection and ADV measurements show that the shedding frequency is independent of height. Whilst we might expect such a result for a cylinder, where the width of the obstacle is constant, it is not clear why this should be the case with a cone or hemisphere. Indeed, for neutral low Reynolds number flow past tall slender cones (e.g. Papangelou 1992) it is known that vortex shedding can occur in cells and in each cell the shedding occurs independently and at a different frequency to adjacent cells. There was no evidence for this type of behaviour in our experiments though it is possible that it may occur for lower values of F_h and/or lower Re than those studied here. Further work (ideally involving the simultaneous use of more than one ADV probe) is required to confirm or disprove this. The fact that in the experiments presented here the shedding frequency is independent of height indicates that a single length scale controls the vortex-street dynamics. Indeed, experiments conducted by Sysoeva & Chashechkin (1988) show that for strongly stratified flows the shape of the wake behind a sphere, defined by the separation lines on the body, is approximately rectangular. In our experiments, however, examination of the dye motion behind the cone C1 reveals that in general this is not the case: the separation lines exhibit a spanwise periodic oscillatory motion,

whose phase depends on height, and the mean position of the separation lines is such that the width of the wake decreases towards the summit. This would appear to be somewhat inconsistent with the fact that the Strouhal number data for both shapes of cone can be made to collapse by choosing a single suitable length scale (see figure 15).

We have investigated this further by performing some additional tows with two shapes of flat plate: a triangular plate of height 250 mm and base width 500 mm (the same cross-sectional shape as the cone C1) and a rectangular plate of height 250 mm and width 200 mm. For such obstacles the separation points are fixed at the edges and thus the initial shape of the wake is determined by the obstacle shape alone. The Strouhal numbers, $S = fL/U$, and $S_2 = fL_2/U$ for the plates are shown in figures 13(*b*) and 14(*b*), respectively. As for the cones and hemispheres there appears to be a tendency for the Strouhal numbers to increase with increasing F_h and the data do not collapse onto the same curve. We have applied the blockage correction to the plate data and, as can be seen from figure 15(*b*), the data again collapse reasonably well. It appears, therefore, that even though the shapes of the wakes immediately behind the obstacles are quite different for the triangular and rectangular plates (and also different to the cones and hemispheres), further downstream a single length scale can define the vortex-street dynamics. In a way these results are consistent with those of Sysoeva & Chashechkin (1988) and suggest that in general, although the separation lines will not describe a rectangular shape, further away from the obstacle the wake may well have this form.

Note that Hunt *et al.* (1997) suggest a different length scale for the width of the wake, namely the summit region width, L_s, i.e. the width of the orography at the dividing-streamline height. If such a length scale were important, we would expect that, after some suitable blockage correction, the Strouhal number based on this length scale would collapse onto the same curve for the different obstacles. For conical and triangular obstacles the width L_s becomes very small at low Froude numbers and, as shown by figure 15(*b*), for the triangular plate, the resulting values of the blockage-corrected Strouhal number, $S_s = fL_s/U_c$, are much smaller than the values of S_{2_c} for both the triangular and rectangular plates. Note that in the definition of S_s, the corrected speed U_c which is used is obtained by replacing L_2 by L_s in equation (4.1). Since for the rectangular plate S_{2_c} and S_s are identical, we conclude that, in this case at least, the width of the summit region is not the relevant length scale.

5. The drag due to vortex shedding and the verge region

5.1. *The vortex-shedding contribution*

As noted in § 4.1, it is not easy to account for the changes in drag (cf. neutral flow at the same Reynolds number) using gravity-wave arguments alone. We have investigated how the vortex-shedding mechanism contributes to the drag by suspending a splitter plate behind the cone C1. The plate, which was slightly higher than the obstacle and approximately 1 m long, was suspended approximately 5 mm to the rear of the cone on the centreline. Flow visualization revealed that the addition of the plate successfully prevented the vortex shedding and the resulting drag coefficient is displayed in figure 17 along with the drag coefficient for the cone without the splitter plate for comparison. For values of $F_h \lesssim 0.3$ the prevention of the vortex shedding in the wake reduces the drag by about 25%. For higher values of F_h the drag appears to be relatively unaffected by the splitter plate. Clearly the vortex-shedding mechanism is a major contributor to the drag for the more strongly stratified flows ($F_h \lesssim 0.3$).

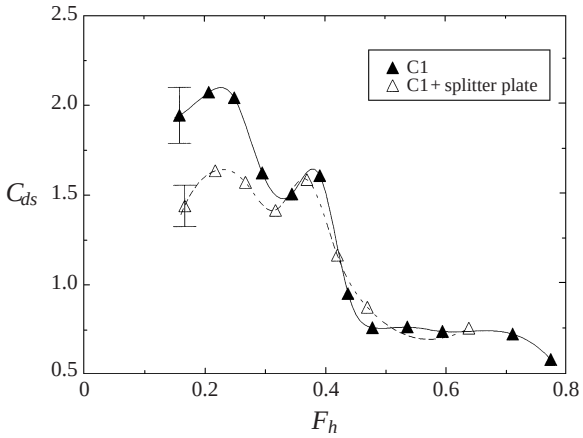

FIGURE 17. The variation of the drag coefficient, C_{ds}, with F_h for the cone C1 with and without a splitter plate attached.

As stated in § 3.2, the drag coefficients for the hemispheres HS1 and HS2 are, like the Strouhal numbers, significantly different. This is particularly true of the drag coefficients at low F_h. Since the blockage ratio can significantly affect the Strouhal number (see § 4.4) we shall attempt to account for blockage effects on C_{ds} also by defining a corrected drag coefficient, C_{ds_c}, as

$$C_{ds_c} = \frac{\overline{\tau}}{\frac{1}{2}\rho U_c^2 A}, \tag{5.1}$$

where U_c is given by equation (4.1). By comparing figure 18, which shows C_{ds_c}/C_d vs. F_{h_c}, with figure 4 it is evident that the effect of such a correction is to reduce the drag from the measured values by a factor of up to about 50%. The agreement between the two hemispheres is perhaps slightly improved at the lower Froude numbers ($F_h \lesssim 0.5$, $F_{h_c} \lesssim 0.75$) by this correction. Note that for all the obstacles C_{ds_c}/C_d tends to values considerably less than unity as F_{h_c} increases. Whilst it is possible that this is due to the fact that the blockage correction used is inappropriate at high values of F_h (since the flow becomes increasingly three-dimensional as F_h increases), Castro *et al.* (1990) also found that $C_{ds}/C_d < 1$ for weak stratification and explained this effect on the basis of the inhibiting effects of the stratification on the vertical motion in the separated wake.

5.2. *The verge-region contribution*

Verge-region effects have been investigated by making a simple modification to the shape of the hemisphere HS1. The modified shape, illustrated in figure 19, was formed by adding an upstream-pointing 'nose' to the hemisphere. The effect of the nose is to stretch the otherwise concentric circular contours below 100 mm in the upstream direction, resulting in semi-ellipses. The variation with height of the semi-major axes of these semi-ellipses is such that the slope of the shape tends to zero at the tip of the 'verge'.

Drag measurements were made for this obstacle for both stably stratified and neutral flow. Results for the neutral case are shown in figure 2(*b*). Despite the increase in skin friction caused by the addition of the verge the drag appears to be reduced by about 20%. This reduction is presumably due to the obstacle's more streamlined

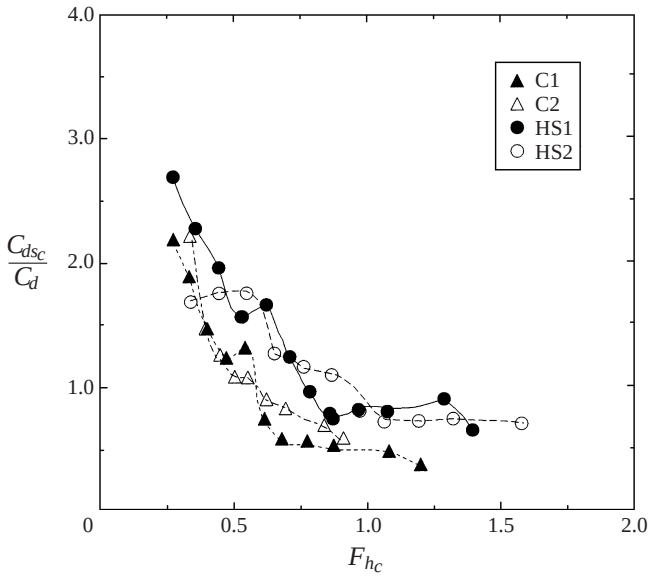

FIGURE 18. The dependence of the ratio of the drag coefficient corrected for blockage, C_{ds_c}, to the neutral drag coefficient, C_d, on the Froude number, F_{h_c}.

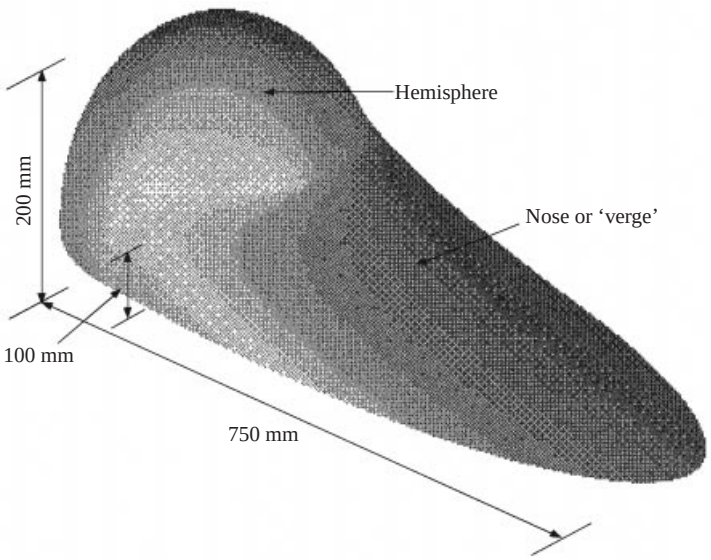

FIGURE 19. The hemisphere HS1 with 'verge' attached. See text for further explanation.

shape which must delay separation and reduce the size of the wake. Figure 20 compares the stratified drag coefficient with and without the verge. It appears that for the very lowest values of F_h, the addition of the verge increases the drag and as F_h increases, the increase in the drag becomes less significant. Greenslade (1994) has shown that the presence of a verge region in stratified conditions will cause vertical motion within the verge region, leading to the possibility of gravity-wave generation, thus increasing the drag. The motion of dye, injected so as to flow over and around the verge, does indeed reveal downward vertical deflections (like those observed in

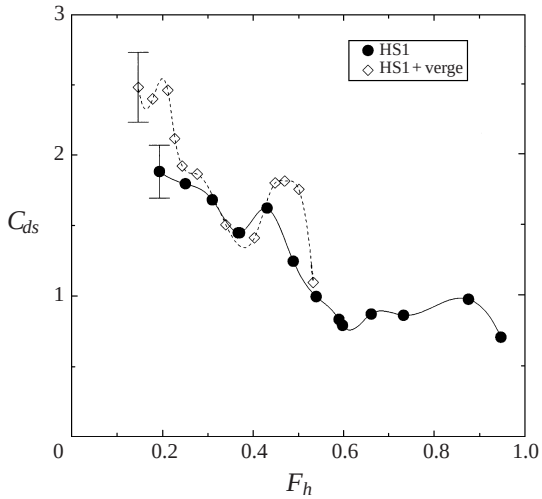

FIGURE 20. The variation of the stratified drag coefficient, C_{ds}, with F_h for the hemisphere HS1 with and without the upstream pointing verge attached.

§4.3) which did not exist in the absence of the verge. However, no significant vertical motion was observed above the verge in the middle region of the flow, indicating that either the direction of gravity-wave propagation away from the verge region is such that the dye visualization was simply in the wrong place, or no gravity waves were generated. At present we are unable to draw any firm conclusions regarding this. There are, of course, factors other than gravity-wave generation which could explain the increase in the drag. The presence of strong stratification may cause an otherwise turbulent boundary layer to be laminar, thus increasing the likelihood of early flow separation and increasing the width of the wake. The verge will also increase skin friction. However, given the reduction in the drag caused by the verge in the neutral case it is likely that this effect will be small.

6. Conclusions

In this study we have addressed some fundamental questions regarding stratified flows past three-dimensional orography. The laboratory experiments have revealed some interesting new results and significant differences between the observed flows and predictions based on Drazin's (1961) theory. For example, the experiments show that the flows are unsteady over a wide range of Froude numbers whereas Drazin's solution is for steady flow. As observed by previous researchers (e.g. Brighton 1978; Castro *et al.* 1983), flow visualization reveals the presence of a separated wake (which itself is not accounted for by the theory) in which vortex shedding occurs. Velocity measurements and flow visualization show that the shedding persists up to values of F_h as high as 0.4. The vortex shedding is also responsible for a spanwise oscillation upstream of the obstacles.

Contrary to the findings of Sysoeva & Chashechkin (1988), the shape of the wake, as defined by the separation lines, is in general not rectangular. However, the frequency of the vortex shedding measured some distance downstream of the orography (typically between $3L$ and $4L$) is independent of height and by defining a Strouhal number based on L_2, the obstacle width at half the dividing-streamline

height, the Strouhal numbers for the cones and hemispheres collapse, to a reasonable degree, onto the same curve when plotted against Froude number. In calculating these Strouhal numbers some allowance for blockage effects must be made. This has been done quite successfully by defining an approximate average velocity based on the idea that the mass flux at the side of the obstacle must equal that upstream (see equation (4.1)). Additional Strouhal number measurements for triangular and rectangular flat plates, again based on L_2 and the blockage-corrected tow-speed, further confirm the collapse of the data and although our suggestion of L_2 as a controlling length scale is no more than an educated guess, the agreement indicates that away from the orography the wake is approximately rectangular even though the separation lines on the surface do not describe such a shape. Note that the length scale L_2 is significantly different to that proposed by Hunt *et al.* (1997) who suggested that the width of the wake is determined by the summit region width, L_s. Our results reveal that, at least in the cases studied here, this is not the case.

The results show that stratification significantly increases the drag above the values in neutral flow. Depending on the obstacle shape the maximum value for the drag is typically between 2.8 and 5.4 times the value in neutral flow when $F_h \lesssim 0.25$. The results also show that, in general, under strongly stratified conditions ($F_h < 1$), as F_h decreases, the drag coefficient increases whilst the wave amplitude decreases. This behaviour is different to what occurs at more moderate stratification where the drag and wave amplitude are closely linked and is clearly inconsistent with the idea that gravity waves are largely responsible for the drag. For very strongly stratified flows the dominant contribution to the drag comes from the presence of a separated wake. Drag measurements for a cone of unit slope with a splitter plate show that vortex shedding alone is responsible for about 25% of the drag when $F_h \lesssim 0.3$. The contribution from the wake to the net drag could well be important at atmospheric scales also, in which case it is important that such effects are properly represented in orographic drag parametrization schemes for numerical weather prediction models. Note that gravity-wave generation still makes a measurable contribution to the drag however, as is evident from the K-dependence of the drag coefficient measurements when $K < 3$. The effect of a verge region on the drag has also been investigated. Although only preliminary, our study indicates that such a region is a likely (but perhaps relatively minor) source of drag in stratified flows, as recent theory suggests.

The authors would like to thank Dr G. Hughes, Dr D. Heist, Professor A. Robins, Mr T. Lawton and Mr A. Wells whose technical assistance and advice proved invaluable during the course of this work. Much of the work was funded by the Natural Environment Research Council under grant GR3/8831 and W. H. S. is grateful to the Engineering and Physical Sciences Research Council for support under grant GR/L26513.

REFERENCES

Baines, P. G. & Hoinka, K. P. 1985 Stratified flow over two-dimensional topography in fluid of infinite depth: a laboratory simulation. *J. Atmos. Sci.* **42**, 1614–1630.

Berlin, P. 1981 Meteosat tracks Kármán vortex streets in the atmosphere. *ESA Bull.* **25**, 16–19.

Brighton, P. W. M. 1978 Strongly stratified flow past three-dimensional obstacles. *Q. J. R. Met. Soc.* **104**, 289–307.

Castro, I. P. & Snyder, W. H. 1993 Experiments on wave breaking in stratified flow over obstacles. *J. Fluid Mech.* **255**, 195–211.

Castro, I. P., Snyder, W. H. & Baines, P. G. 1990 Obstacle drag in stratified flow. *Proc. R. Soc. Lond.* A **429**, 119–140.

Castro, I. P., Snyder, W. H. & Marsh, G. L. 1983 Stratified flow over three-dimensional ridges. *J. Fluid Mech.* **135**, 261–282.

Chomaz, J. M., Bonneton, P. & Hopfinger, E. J. 1993 The structure of the near wake moving horizontally in a stratified fluid. *J. Fluid Mech.* **254**, 1–21.

Drazin, P. G. 1961 On the steady flow of a fluid of variable density past an obstacle. *Tellus* **13**, 239–251.

Greenslade, M. D. 1994 Strongly-stratified airflow over and around mountains. In *Stably Stratified Flows: Flow and Dispersion over Topography* (ed. I. P. Castro & N. J. Rockliff). Oxford.

Hunt, J. C. R., Feng, Y., Linden, P. F., Greenslade, M. D. & Mobbs, S. D. 1997 Low Froude number stable flow past mountains. *Il Nuovo Cimento* **20**, 261–272.

Hunt, J. C. R. & Snyder, W. H. 1980 Experiments on stably and neutrally stratified flow over a model three-dimensional hill. *J. Fluid Mech.* **96**, 671–704.

Huppert, H. E. & Miles, J. W. 1969 Lee waves in a stratified flow. Part 3. Semi-elliptical obstacle. *J. Fluid Mech.* **55**, 481–496.

Lin, Q., Lindberg, W. R., Boyer, D. L. & Fernando, H. J. S. 1992 Stratified flow past a sphere. *J. Fluid Mech.* **240**, 315–354.

Lofquist, K. E. B. & Purtell, L. P. 1984 Drag on a sphere moving horizontally through a stratified liquid. *J. Fluid Mech.* **148**, 271–284.

Long, R. R. 1953 Some aspects of the flow of stratified fluids. I. A theoretical investigation. *Tellus* **5**, 42–58.

Lott, F. & Miller, M. J. 1997 A new subgrid-scale orographic drag parametrization: Its formulation and testing. *Q. J. R. Met. Soc.* **123**, 101–127.

Maskell, E. C. 1965 A theory of the blockage effects on bluff bodies and stalled wings in a closed wind tunnel. *Aero. Res. Counc.* R & M 3400.

Mason, P. J. 1977 Forces on spheres moving horizontally in a rotating stratified fluid. *Geophys. Astrophys. Fluid Dyn.* **8**, 137–154.

Miranda, P. M. A. & James, I. N. 1992 Nonlinear three-dimensional effects on gravity wave drag: Splitting flow and breaking waves. *Q. J. R. Met. Soc.* **118**, 1057–1081.

Paisley, M. F. & Castro, I. P. 1995 Numerical computations of stratified flow over three-dimensional obstacles. *Numerical Methods for Fluid Dynamics V* (ed. K. W. Morton & M. J. Baines) pp. 523–531. Clarendon.

Palmer, T. N., Shutts, G. J. & Swinbank, R. 1986 Alleviation of a systematic westerly bias in general circulation and numerical weather prediction models through an orographic gravity-wave drag parametrisation. *Q. J. R. Met. Soc.* **112**, 1001–1039.

Papangelou, A. 1992 Vortex shedding from slender cones at low Reynolds numbers. *J. Fluid Mech.* **242**, 299–321.

Peltier, W. R. & Clark, T. L. 1979 The evolution and stability of finite-amplitude mountain waves. Part II: Surface wave drag and severe downslope windstorms. *J. Atmos. Sci.* **36**, 1498–1529.

Rottman, J. W. & Britter, R. E. 1986 The mixing efficiency and decay of grid-generated turbulence in stably-stratified fluids. *Proc. 9th Australasian Fluid Mech. Conf.*, Dec. 8–12, pp. 218–221. Univ. Auckland, Auckland, N.Z.

Rottman, J. W., Broutman, D. & Grimshaw, R. 1996 Numerical simulations of uniformly stratified fluid flow over topography. *J. Fluid Mech.* **306**, 1–30.

Schar, C. & Durran, D. R. 1997 Vortex formation and vortex shedding in continuously stratified flows past isolated topography. *J. Atmos. Sci.* **54**, 534–554.

Scinocca, J. F. & Peltier, W. R. 1994 The instability of Long's stationary solution and the evolution toward severe downslope windstorm flow. Part II: the application of finite-amplitude local wave-activity flow diagnostics. *J. Atmos. Sci.* **51**, 623–653.

Sheppard, P. A. 1956 Airflow over mountains. *Q. J. R. Met. Soc.* **75**, 528–529.

Smith, R. B. 1988 Linear theory of stratified flow past an isolated mountain in isosteric coordinates. *J. Atmos. Sci.* **45**, 3889–3896.

Smith, R. B. 1989 Mountain-induced stagnation points in hydrostatic flow. *Tellus* **41A**, 270–274.

Smith, R. B., Gleason, A. C. & Gluhosky, P. A. 1997 The wake of St. Vincent. *J. Atmos. Sci.* **54**, 606–623.

Smolarkiewicz, P. K. & Rotunno, R. 1989 Low Froude-number flow past 3-dimensional obstacles. Part I: Baroclinically generated lee vortices. *J. Atmos. Sci.* **46**, 1154–1164.

Snyder, W. H., Britter, R. & Hunt, J. C. R. 1980 A fluid modeling study of the flow structure and plume impingement on a three-dimensional hill in stably stratified flow. *Proc. 5th Int. Conf. on Wind Engng* (ed. J. E. Cermak), pp. 319–329. Pergamon.

Snyder, W. H. & Castro, I. P. 1999 Acoustic-Doppler-Velocimeter evaluation in a stratified towing tank. *J. Hyd. Engng* **125**.

Snyder, W. H. & Hunt, J. C. R. 1984 Turbulent diffusion from a point source in stratified and neutral flows around a three-dimensional hill – II. Laboratory measurements of surface concentrations. *Atmos. Environ.* **18**, 1969–2002.

Snyder, W. H., Thompson, R. S., Eskridge, R. E., Lawson, R. E., Castro, I. P., Lee, J. T., Hunt, J. C. R. & Ogawa, Y. 1985 The structure of strongly stratified flow over hills: dividing-streamline concept. *J. Fluid Mech.* **152**, 249–288.

Sysoeva, E. Y. & Chashechkin, Y. D. 1988 Spatial structure of a wake behind a sphere in a stratified liquid. *J. Appl. Mech. Tech. Phys.* **5**, 655–660.

Trischka, J. W. 1980 Cone models of mountain peaks associated with atmospheric vortex streets. *Tellus* **32**, 365–375.